PCCP

PAPER

View Article Online
View Journal | View Issue

Cite this: *Phys. Chem. Chem. Phys.*, 2019, **21**, 1587

Received 12th October 2018,
Accepted 19th December 2018

DOI: 10.1039/c8cp06368k

rsc.li/pccp

Radiative cooling of cationic carbon clusters, C_N^+, N = 8, 10, 13–16

F.-Q. Chen,[a] N. Kono,[b] R. Suzuki,[b] T. Furukawa,[b] H. Tanuma,[b] P. Ferrari,[c] T. Azuma,[d] J. Matsumoto,[e] H. Shiromaru,[e] V. Zhaunerchyk[f] and K. Hansen *[fg]

The radiative cooling of highly excited carbon cluster cations of sizes N = 8, 10, 13–16 has been studied in an electrostatic storage ring. The cooling rate constants vary with cluster size from a maximum at N = 8 of 2.6 × 10^4 s^{-1} and a minimum at N = 13 of 4.4 × 10^3 s^{-1}. The high rates indicate that photon emission takes place from electronically excited ions, providing a strong stabilizing cooling of the molecules.

I. Introduction

The stability of molecules and clusters against unimolecular decomposition plays an important role in the dynamics and the chemical composition of any gas or plasma at low densities. When collision frequencies become comparable to and smaller than reciprocal dissociation times of excited species, all collisions that form molecules will, by energy conservation, create them with enough excess energy to ultimately cause dissociation, unless the excess energy is dissipated through other non-collisional channels.

Radiative cooling provides one such dissipation channel. The amount of energy that must be carried away by photons to provide absolute stabilization of a collision complex is on the order of the thermal energy of the molecules before formation of the compound. At the same time the internal excitation energy is never less than the formation energy, which is often fairly large compared with thermal energies, implying that only a small fraction of the total energy of the complex needs to be removed to stabilize it. For molecules formed by reactions between smaller molecules and/or atoms with absent or essentially frozen vibrational motion, the energy necessary to quench dissociation is on the order of Boltzmann's constant times the ambient temperature, an energy that can be dissipated by emission of a single photon of an electronic transition or possibly even by a vibrational transition.

The molecular-specific radiative quenching rate therefore becomes an important factor in determining the survival probability of any molecule formed in collisions.[1] The situation is particularly extreme in astrophysical context, where collision frequencies can be less than nHz between the numerous different molecular species now known to exist in space.[2] This environment also produces the still poorly understood infrared emission bands, often assigned to polycyclic aromatic hydrocarbon molecules,[3] which is of obvious interest in the context of radiative cooling processes. Radiation may, for example, play an important role in stabilizing intermediate products in the chain of processes through the top-down mechanism suggested in ref. 4 to be responsible for interstellar C_{60} production. The increasing list of molecular species found in space,[5,6] many of them either carbon based or with a carbon backbone that opens up the possibility for unrestricted molecular growth, makes the question about the molecular survival influenced by radiative cooling particularly relevant.

Of the possible photon emission processes, photons appearing from thermally populated electronic states, in processes known as recurrent fluorescence,[7–9] will for some molecules be the most efficient energy dissipation. Compared to the alternative thermal radiation by vibrational transitions, recurrent fluorescence radiation rates are on one hand reduced by the equivalent of the Boltzmann factor which suppresses the population of the emitting state, but are on the other hand enhanced by an oscillator strength for photon emission from these states which is usually much higher than that of vibrational transitions. The balance between these two factors is tipped toward enhancement of photon emission from the low-lying electronic states. This will

[a] *School of Materials Science and Engineering, Tianjin University, Tianjin 300350, China*
[b] *Department of Physics, Tokyo Metropolitan University, 1-1 Minamiosawa, Hachiouji-shi, Tokyo 192-0397, Japan*
[c] *Laboratory of Solid State Physics and Magnetism, KU Leuven, 3001 Leuven, Belgium*
[d] *Atomic, Molecular & Optical Physics Laboratory, RIKEN, 2-1, Hirosawa, Wako-shi, Saitama 351-0198, Japan*
[e] *Department of Chemistry, Tokyo Metropolitan University, 1-1 Minamiosawa, Hachiouji-shi, Tokyo 192-0397, Japan*
[f] *Department of Physics, University of Gothenburg, 41296 Gothenburg, Sweden*
[g] *Center for Joint Quantum Studies and Department of Physics, Tianjin University, Tianjin 300350, China. E-mail: KlavsHansen@tju.edu.cn*

tend to make radicals, with their lower lying states, more likely to emit radiation with high rates, tending to reverse the fitness pattern for molecular survival which is based on considerations of the higher binding energies of closed shell molecules.

Several species have been established as recurrent fluorescence coolers, both fullerenes,[10–14] smaller carbon clusters,[15–18] carbon-based molecules,[19–22] and metal[23–26] and semiconductor[27,28] clusters. Anionic carbon clusters and molecules tend to have radiative cooling times on the order of tens or hundred microseconds to milliseconds. The cooling of small pure carbon cluster cations is much less known. Only the fullerenes of sizes N = 48–70, 76 have been investigated.[10,12] We report here a study of the radiative properties of cationic carbon clusters of sizes N = 8, 10, 13–16, produced in a high temperature cluster source and measured at the Tokyo Metropolitan University electrostatic storage ring (TMU E-ring).

II. Experimental procedure

A schematic figure of the storage ring used is shown in Fig. 1. The clusters were produced in a laser ablation source with a 532 nm wavelength pulse from a YAG laser ablating a graphite surface. The ions, which were generated without gas cooling and therefore can be expected to be very highly excited vibrationally, were extracted by a pulsed field and further accelerated by a static electric field to a terminal kinetic energy of 15 keV, followed by an injection into the 7.736 m circumference storage ring[29] where they circulated. At injection, a set of bending electrodes (at point A in Fig. 1) was briefly switched off to allow passage from the source line into the ring. After storage was accomplished, the cluster size of interest was selected by pulsing the deflection plates.

The decays were measured time-resolved turn-by-turn in a neutral particle detector at point C at the end of the straight section (around point B in Fig. 1). The detector thus monitored the quasi-instantaneous decay rate of the stored species. The signal comprises all channels that emit neutral massive particles, irrespective of whether the emitted particles are atoms or molecules. Since radiative cooling quenches all non-radiative decays equally indiscriminately, the measured rates provide a faithful representation of the stabilizing effect of the radiation without the need to specify the decay channel. After measurements, the ions were dumped before a new bunch was injected.

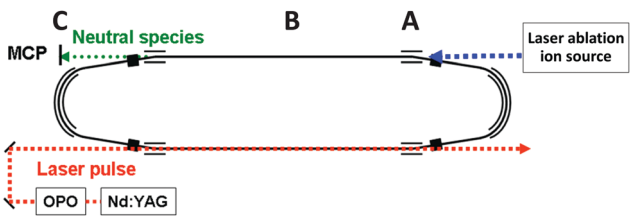

Fig. 1 A schematic drawing of the TMU electrostatic storage ring (TMU E-ring). The ions are produced in the laser ablation source to the right, introduced into the ring at point A. The neutral fragments that are produced by decays in the straight section labeled B are detected with the neutral particle detector at point C.

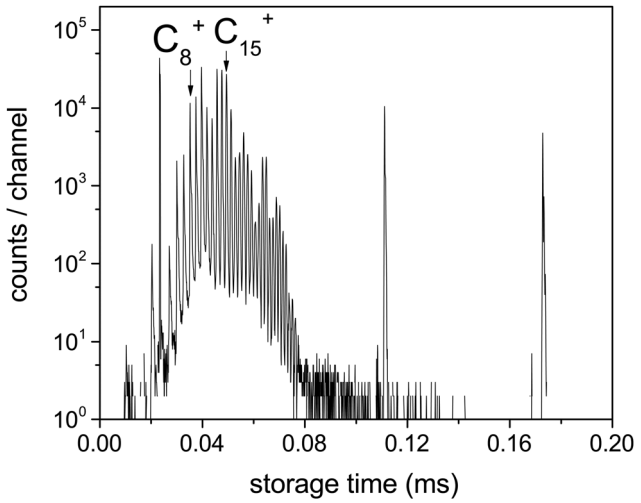

Fig. 2 The neutral counts for the first two hundred microseconds after injection of ions into the ring. The first mass selection pulse was applied between 80 and 110 μs, selecting C_{15}^+ in this case. The peaks appearing before the 80 μs mass selection time are therefore proportional to both the number of ions in the beam and the efficiency of producing neutrals after laser excitation of these ions. The peaks below 80 μs are separated by one carbon mass. Two mass peaks in the first turn in the ring after injection and before mass selection are indicated. The large peak between C_3^+ and C_5^+ is electronic noise.

The laser was fired within 1 ms of injection. Fig. 2 shows the spontaneous decay spectrum for the first few turns in the ring, with mass selection of, in this case, the N = 15 cluster. The spectrum prior to mass selection represents decay rates that are shaped by the combined effects of ion abundances, dissociation energies, internal energy distributions, radiative cooling and possibly also stray counts from grazing collisions with the chamber walls. Because decay rates and not populations are measured here, a direct comparison of the spectrum in Fig. 2 with ion abundance spectra, even produced by similar methods, as in *e.g.* ref. 30, is therefore not possible.

Both spontaneous and laser induced decays were measured in the experiments. For the measurements of the photon induced decay, a 10 Hz tunable OPO laser was used to excite the clusters. The geometry gives measurements of the decay rates at times $(n + 1/2)t_c$ after the laser pulse, where $t_c = 15.8\ \mu s\sqrt{N}$ is the ion circulation time in the ring, and n is a non-negative integer. The number of ion injection/dumping cycles varied from 1.8×10^4 for the most intense beam of C_{15}^+ to above 2×10^5 for C_{10}^+. Fig. 3 shows examples of unimolecular decay spectra observed in the ring after mass selection of C_{15}^+ without and with a laser pulse. The laser power was monitored continuously. The highest pulse energy was 2.2 mJ per pulse, used at 520 nm on N = 15. Most of the wavelengths were chosen so the photon energies were high enough to cause a zero value of the t_0 that appears in eqn (5), which was indeed found to be the case in the data analysis. This simplifies the data analysis but has no fundamental consequences. For N = 8 the choice was dictated by the photon absorption cross section. For N = 15, different wavelengths were used for the purpose of

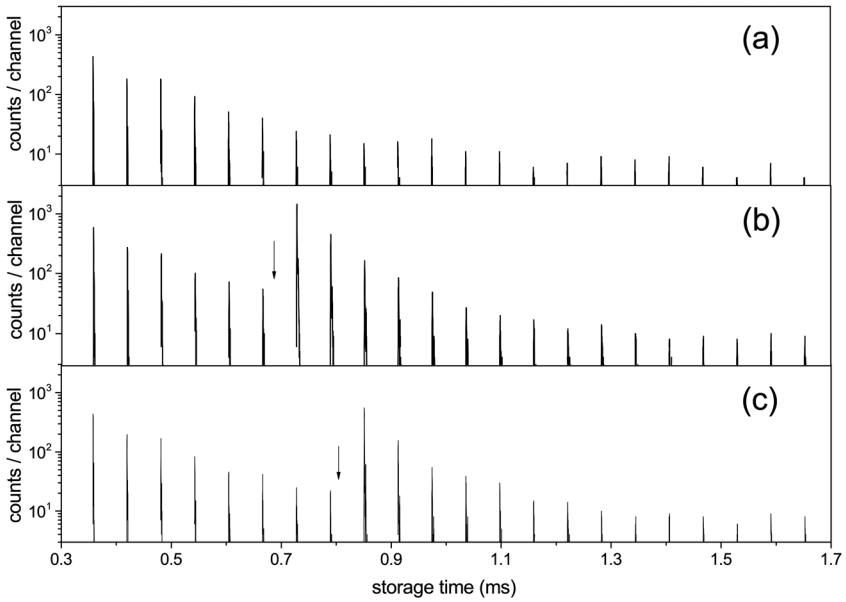

Fig. 3 The C_{15}^+ spectrum (a) without laser excitation, (b) with photon energy 2.58 eV (λ = 480 nm) fired at times 0.682 ms, with the first enhanced ion signal detected at 0.729 ms, and (c) $h\nu$ = 2.00 eV (λ = 620 nm) with the laser fired at 0.805 ms and the first enhanced peak appearing at 0.851 ms. Laser firing times are indicated by the vertical arrows. The laser is fired in one straight section of the ring and the neutral decay products are detected in the other, which causes one half turn delay between the laser pulse and the detected signal. An additional small delay, about a quarter of a period, in the detection is introduced by the travel time from the decay section to the detector (B to C in Fig. 1).

checking that the width of the excitation energy distribution was sufficiently broad to accommodate the special features used in the data analysis below.

III. Experimental results

For all clusters both the laser induced decays and the spontaneous decays of the hot clusters produced in the source were used to extract the cooling times. The photon energies used were $h\nu$ = 2.38 eV (λ = 520 nm) for N = 10, 13, 14, 15, 16, $h\nu$ = 2.58 eV (λ = 480 nm) for N = 15, $h\nu$ = 2.00 eV (λ = 620 nm) for N = 15, and $h\nu$ = 1.98 eV (λ = 625 nm) for N = 8. For N = 15, all of pulse energies, photon energies and laser firing times were varied. All the measured photon enhanced decay profiles were found to be identical, in the sense that the time dependence of the enhanced decay did not change with these parameters. This indicates that the enhanced signal is not shaped by source conditions but reflects intrinsic properties of the clusters. Furthermore, if the observed decay of the enhanced signal would be governed by the unimolecular rate constant, it should depend on the laser light wavelength and on the internal energies before excitation, effectively the storage time before laser excitation. However, this is seen experimentally not to be the case, and the disappearance of the signal after laser excitation cannot therefore be ascribed to the energy dependence of the rate constant k_a. These conclusions agree with those drawn from previous experiments with the same apparatus on cooling of anions,[14,31–33] and with a number of similar studies from other experimental facilities, see for example ref. 12, 13, 21, 22, 24, 26 and 34–37. Finally, as will be clear below, conclusions about the cooling rates do not depend on the precise number of photons absorbed, although we expect that most of the signal is due to single photon absorption.

For all photon-induced decay, the enhanced decays were calculated from the data by subtraction of a reference laser-off spectrum, normalized to identical pre-laser counts to compensate for the (minor) fluctuations in the source intensity. The source has previously been tested in detail for stability with respect to the decay time profile of C_{60}^-, and it was found that although intensities could vary, the time profile of the signal had a very stable shape.[14] This is consistent with the behavior observed here in the reference spectra and was assumed in the analysis. Examples of an integrated spectrum with and without laser enhancement is shown in Fig. 4.

Special consideration was paid in the analysis of the peak intensities to the possibility that the clusters could contain one or several hydrogen atoms, because hydrogen addition can change the radiative properties dramatically.[15] The geometry of the laser overlap did not allow selective excitation of molecules differing in mass by 1 u, but the detected peaks are separated to a degree that it is possible to integrate intensities of ions differing by 1 u separately. Cooling times were found to be identical for the observable peaks corresponding to all-^{12}C clusters and those 1 u higher. These higher mass clusters can therefore be assigned to clusters containing one ^{13}C atom, and any presence of hydrogenated species is small enough to not affect the measured values.

IV. Analysis

In the absence of an external cooling gas in the source, the laser ablation produces clusters with broad excitation energy

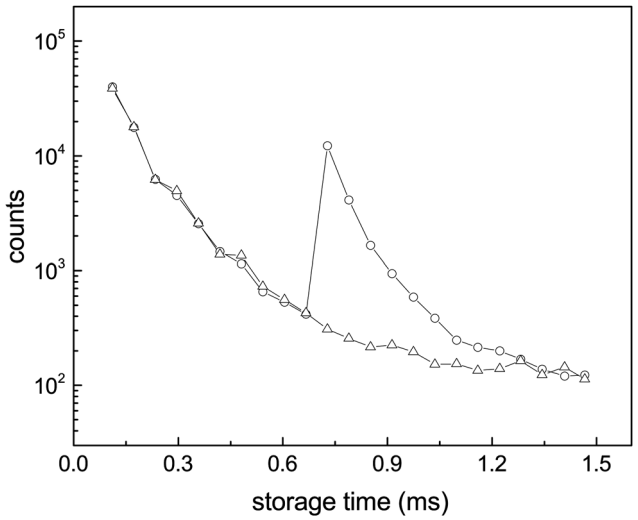

Fig. 4 Enhanced decays of the N = 15 cluster after photon absorption. The data points are the integrals of the peaks in the spectra (a and b) of Fig. 3. The wiggles seen most clearly before the laser pulse are caused by the so-called betatron oscillations. The depletion of the number of the stored ions by laser irradiation is not discernible.

distributions. The highest excitation energies are sufficient to cause spontaneous unimolecular decay of the clusters in the storage ring, and most likely also during transfer from the source to the ring, although this is not directly observable. Decay from such an ensemble occurs as

$$I = \int_0^\infty g(E) k_a(E) e^{-k_a(E)t} dE, \quad (1)$$

where $g(E)$ is the distribution of excitation energies the cluster gains in the source. The decay occurs from the clusters with the energy for which the integrand in eqn (1) peaks. Under fairly mild conditions on both $g(E)$ and the energy dependence of the unimolecular rate constant $k_a(E)$, this can be approximated by a power law

$$I \propto \frac{1}{t}. \quad (2)$$

The phenomenon, which has been observed and discussed in details on a number of occasions, see *e.g.* ref. 34, 38 and 39, must generally be expected to appear whenever decay rates are averages over broad distributions of single exponential decays, in particular for thermally activated processes of molecules with broad internal energy distributions.

The presence of a power law decay rate, *vs.* the naively expected exponential decay, is essential for the observation of the radiative quenching, as was already noted in ref. 10 and 38. Radiative cooling will cause a deviation from this $1/t$ profile by reintroducing an exponential suppression of the decay at long times.[34] For a few examples of previous applications of the technique, please see ref. 12–14 and 39 for fullerene studies, and ref. 19–22 for studies of carbon-based molecules.

The precise interpretation of such a radiatively quenched decay depends on the energy of the emitted photons. To reduce the unimolecular decay by the factor exp(1) or more, the photon energies need to exceed the value determined by

$$h\nu \frac{d \ln k_a}{dE} \gtrsim 1, \quad (3)$$

where k_a is the unimolecular decay constant. A conservative estimate of the left hand side of this equation, which involves the unimolecular frequency factors and activation energies, gives a required photon energy exceeding 0.5 eV. The cooling rates will turn out to be much higher than those given by vibrational transitions,[40] strongly indicating that the radiation originates in excited electronic states. It is therefore most likely that photon energies exceed the limit in eqn (3) and the emission of a single photon quenches any further unimolecular decay. The 0.5 eV criterion will also be fulfilled by all the transitions found in the quantum chemical calculations presented below, with the exception of a very weak transition for each of the clusters N = 15 and N = 16.

Proceeding with the one-photon radiative quenching of the unimolecular decays, the decay rates are to a good approximation given by[33]

$$I \propto \frac{e^{-k_p(t-t_{las})}}{t - t_{las}}, \quad (4)$$

where I is the measured neutral signal, which is equal to the decay rate apart from instrumental factors, k_p is the rate constant of photon emission, and t_{las} is the laser firing time. A similar equation without t_{las} holds for the clusters produced sufficiently hot in the source to undergo spontaneous decay.

In addition to the quenching by radiative cooling, deviations from a pure power law after photo-excitation could also be caused by a photon energy that is too small to shift the energy distributions sufficiently high in energy to cause a $1/t$ decay.[14] Such a situation will give a decay with a shifted zero time, t_0 (see ref. 14 for an application, and the theoretical justification in ref. 41)

$$I \propto \frac{e^{-k_p(t-t_{las}+t_0)}}{t - t_{las} + t_0}, \quad (5)$$

where t_0 is a constant which only depends on the photon energy for a given cluster. Fitting the curves gave values of t_0 consistent with zero in all cases. Also this question depends on the heat capacity and the photon energies used. A comparison of these quantities with those observed for the much larger C_{60}^- in ref. 14 corroborates that the already fairly small values of t_0 for that molecule will here be so small that they can safely be ignored.

The suppression of the decay by radiative cooling is conveniently extracted by plotting the product of the enhanced count rate and the time elapsed after the photon absorption as a function of time after the photon absorption, as $(t - t_{las})I(t - t_{las}) \propto \exp(-k_p(t - t_{las}))$ *vs.* $t - t_{las}$ for the laser based decays, and as $tI(t) \propto \exp(-k_p t)$ *vs.* t for the spontaneous decay. Fig. 5 shows this plot for all measured clusters sizes for

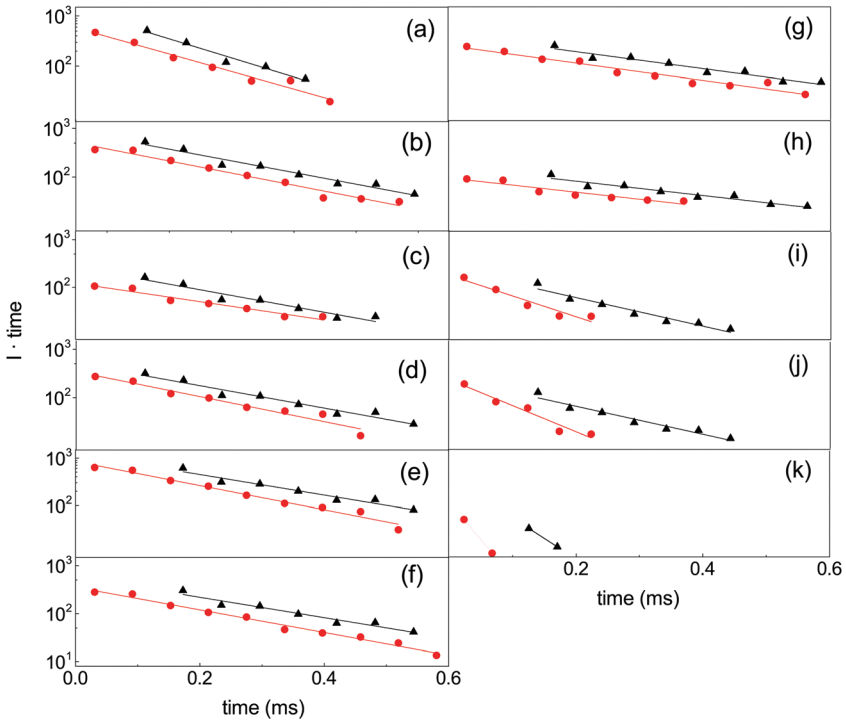

Fig. 5 The product of unimolecular decay count rate and time elapsed after photon absorption (red circles), and the spontaneous decay (black triangles). The time that appears as the abscissa and in the ordinate as a multiplicative factor on the measured intensities is the time after laser excitation (for red circles) and the time after production in the source (black triangles). The frames give the data for (a) C_{16}^+ (520 nm, 0.4335 ms); (b) C_{15}^+ (480 nm, 0.7278 ms); (c) C_{15}^+ (620 nm, 0.8511 ms); (d) C_{15}^+ (480 nm, 0.8511 ms); (e) C_{15}^+ (480 nm, 0.7278 ms); (f) C_{15}^+ (520 nm, 0.7278 ms); (g) C_{14}^+ (520 nm, 0.8826 ms); (h) C_{13}^+ (520 nm, 0.7916 ms); (i) C_{10}^+ (520 nm, 0.6942 ms); (j) C_{10}^+ (520 nm, 0.7444 ms); (k) C_8^+ (625 nm, 0.2152 ms). The spectra (b and e) were recorded with different digital resolution (100 ns and 200 ns, respectively).

both the laser enhanced peaks and the spontaneous decay from the source.

The curves are well fitted by an exponentially decreasing function, from which the photon emission rate constants k_p are extracted directly. The good fits, which seem only to suffer from the betatron oscillations, confirm very convincingly the basis of analysis, *viz.* the presence of broad energy distributions and the concomitant power-law decay suppressed by radiative cooling. The values extracted from the source-produced decay and the photon enhanced signal are also in good agreement for $N = 13$, 14, 15, 16. Some difference between the two is seen for $N = 10$ and a more pronounced difference for $N = 8$, where slightly less than a factor of two separates the two. The differences for $N = 8$, 10 may be ascribed to the presence of high energy emitting states. Such states will be more sensitive to the excitation energy (temperature) than states at lower energies. Their presence cannot be confirmed from these data alone, but the quantum chemical calculations explained below do in fact give the two highest photon energy threshold for precisely $N = 8$ and $N = 10$ (0.95 eV and 0.60 eV, respectively). Although the spontaneous and light-induced rate constants for these two cluster sizes differ, we note that the variation is relatively small compared to the size dependence of the rate constants and we will use an average in the following. The values of k_p are shown in Fig. 6. The five measured values of the spontaneous and the light-induced decay for $N = 15$ gave averages of $(4.6 \pm 0.3) \times 10^3\ s^{-1}$

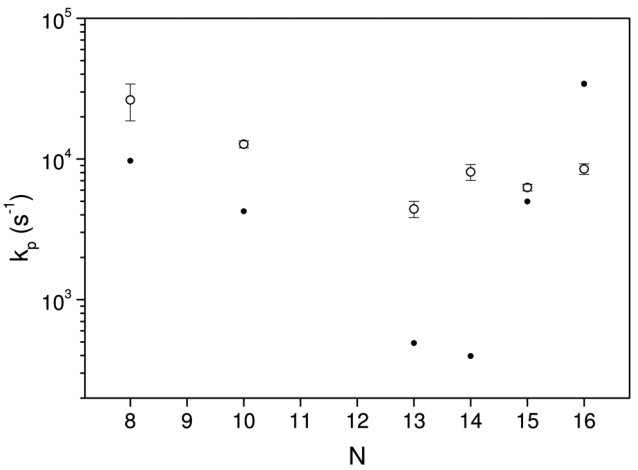

Fig. 6 The fitted values of k_p for the different clusters measured in the experiments. The data are averaged over laser fluences and firing times, and include the lifetimes determined from the spontaneous decays. The error bars are statistical 1σ values. The filled circles are the theoretical values, calculated as described below.

for the spontaneous decay and $(6.6 \pm 0.2) \times 10^3\ s^{-1}$ for the light-induced decay. The errors given are those of the mean values.

Since the radiative and unimolecular decay processes occur in parallel in the measurements, the measured radiative time constants correspond to the energy where the unimolecular

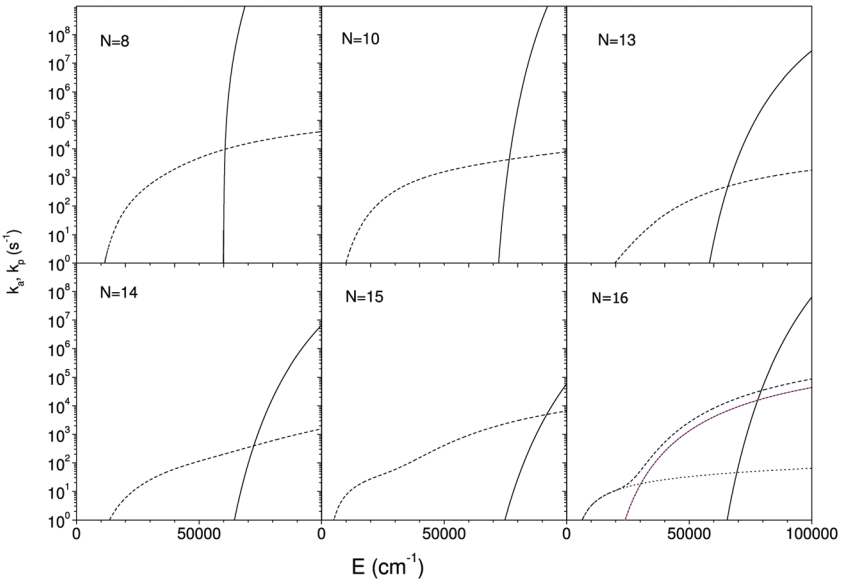

Fig. 7 The calculated unimolecular and radiative rate constants, calculated as described in the main text. The full lines are the unimolecular rate constants, and the short dashed lines the total photon emission rate constants. The dotted lines in the frame for $N = 16$ are the contributions from the three lowest excited states. Only two appear visible because the two highest yield curves are degenerate. The measured radiative emission constant equals the value at the crossing point of the two decay curves.

decay constant, $k_{a,N}$, and the radiative time constant are on the same order (see also Fig. 7);

$$k_p(E) \sim k_{a,N}(E). \quad (6)$$

In order to find both the energy and compare with theoretical expectations, these two rate constants need to be calculated. The general expression for photon emission from a single level with energy $h\nu$ above the electronic ground state is,[39,42]

$$k_p = A\frac{\frac{\rho(E-h\nu)}{\rho(E)}}{1-\frac{\rho(E-2h\nu)}{\rho(E-h\nu)}}, \quad (7)$$

where A is the Einstein A-coefficient of the state, and ρ is the level density of the unfragmented cluster at the energies indicated. The level densities are well approximated by the vibrational contribution alone. For electronic transitions with their high $h\nu$, the ratio in the denominator can often be ignored. We will retain it in view of the high energies here.

As is clear from the argument of the numerator in the expression, the photon emission rate constant represents a (microcanonically) thermally activated process. In principle this energy dependence of the photon emission process should be included into the calculation of the time profile that leads to eqn (4). The variation with excitation energy is, however, slow when compared with the unimolecular rate constant and it can be ignored without any major loss of precision. Appendix II shows this by an explicit calculation of the first order contribution of a finite slope of the photon emission *vs.* cluster excitation energy.

The observed photon emission rate constants include contributions from all possibly excited states and from both linear and ring conformers. The theoretical rate constants were calculated as the average over all emitting states, with energies $h\nu_i$ and spontaneous emission rate constants A_i-coefficients

$$k_p = \sum_i A_i\frac{\frac{\rho(E-h\nu_i)}{\rho(E)}}{1-\frac{\rho(E-2h\nu_i)}{\rho(E-h\nu_i)}}. \quad (8)$$

The relevant optical properties have not been measured. The spectra in ref. 43 do include the C_8^+, but only at much higher energies than relevant here. To find the quantities that enter this equation, a series of density functional theory (DFT) calculations were therefore performed. The vibrational quantum energies were calculated using the wB97X-D3 exchange–correlation functional and the Def2-SVP basis set, as implemented in the ORCA 4.0.1 software package.[44] The properties of the electronically excited states were calculated by time-dependent DFT (TDDFT) using the same level of theory. All the electrons of carbon were included in the calculations. In addition, dissociation energies of all possible fragmentation channels were calculated. The applied level of theory was tested by its prediction of the correct lowest-energy isomer for each cluster size,[45] as well as by the calculated dissociation channels. Vibrational frequencies were computed for all sizes and conformers, which were used to calculate level densities. The vibrational analysis was performed with the M062X functional and cc-pVTZ basis set from the Gaussian 16 package.[46] For calculations of linear clusters, molecular symmetry constraints were implemented in order to obtain the correct number $3N - 5$ of vibrational modes. Finally, also the energies and oscillator strengths of the three lowest excited states were calculated.

All cluster sizes calculated, N = 8 to 16, are rings in their lowest energy state. For N = 8, 9 the linear isomer ground state energy is between 0.8 eV and 0.9 eV above the ground state ring energy, whereas for the larger clusters the gap exceeds 2.1 eV, reaching 3.4 eV for C_{16}^+. These values are, apart from N = 10, consistent with ion mobility experiments,[47] which observed the co-existence of rings and linear structures up to N = 10 and rings exclusively for larger cationic clusters. In that experiment the clusters are formed hot but quenched with a cooling gas, which may open the possibility that the structures are not sampled from entirely equilibrated thermal distributions. This will distort the comparison with the values calculated here. The lowest energies of the three optically active states calculated were 0.95 eV for N = 8; 0.60 eV for N = 10; 0.46 eV for N = 13; 0.46 eV for N = 14; 0.19 eV for N = 15; 0.18 eV for N = 16. All of these are therefore within reach of thermal excitation.

The lowest energy channels are in all cases the loss of a neutral carbon trimer:

$$C_N^+ \rightarrow C_{N-3}^+ + C_3. \quad (9)$$

The decay channels agree with previous measurements of these species.[48–54] The calculated dissociation energies are D_8 = 6.75 eV, D_{10} = 8.37 eV, D_{13} = 5.73 eV, D_{14} = 6.02 eV, D_{15} = 6.86 eV, and D_{16} = 6.62 eV.

The rate constants for these are calculated with the detailed balance equation[42]

$$k_{a,N} \approx Z_3(T_d)\frac{m}{\pi^2\hbar^3}\langle\sigma\rangle T_d^2\frac{\rho_{N-3}(E-E_a)}{\rho_N(E)}, \quad (10)$$

where $Z_3(T_d)$ is the rotational partition function of the small fragment at the microcanonical product temperature T_d, m is the reduced mass of the decay channel, and $\langle\sigma\rangle$ is the temperature-averaged attachment cross section in the inverse process. In principle also the electronic degeneracies should be included into this expression, but they will not make any major difference in the analysis. Some details of the calculation of this rate constant are given in Appendix I.

The calculated rate constants and photon emission rate are shown in Fig. 7. Only the radiation from the ring structures are included in the radiative rate constants, which are the sums of the three lowest optically excited states. The linear structures have generally significantly higher oscillator strengths than the ring structures, and the inclusion of radiation from linear structures will for most of the clusters give an extremely poor agreement with the experimental data.

V. Discussion

The radiative cooling of hot cationic carbon cluster observed in this work proceeds with very high rate constants that are only consistent with emission from thermally excited electronic states. The quantum mechanical calculations of the oscillator strengths and energies of such states do not agree well with the data, yielding emission rate constants that range more than two orders of magnitude from the lowest to the highest, whereas the experimental data cover less than an order of magnitude around 10^4 s^{-1}. As such the theory can not be said to reproduce the experimental results.

We do note, however, that the theoretical results bracket the experimental, with values both above and below the experimentally measured. We also note that any reasonable agreement requires that the linear conformers are excluded from the calculation of the optical rate constants, in spite of the fact that these states are not the lowest conformers, and that the opening of a ring requires an activation energy, in addition to the energy needed to excite the ion to the emitting electronic states. This leads to a strongly reduced population, but not sufficient to compensate for the much higher oscillator strength of these doubly excited states.

The exclusion of the linear conformers is entirely *ad hoc* and we can only speculate why this exclusion is necessary to obtain a semblance of agreement between theory and experiment. One possibility is that strong geometric deformations caused by the very highly excited vibrational states could push electronically excited state energies up and/or reduce thermally averaged oscillator strengths. In hot source productions the temperatures of the decaying clusters are determined by the dominant decay channel activation energies. In the present case the calculated values range between 5.89 and 8.54 eV. This gives (equivalent, or microcanonical) temperatures of the decaying ions often exceeding 4000 K, opening the possibility of exploring vastly larger parts of the phase space than the two conformers observed at low temperatures.

The theory-experiment deviations do not seem to correlate simply with the magnitude of the dissociation energy, but there is indeed a weak correlation between measured values of k_p and calculated dissociation energies, with a tenfold increase in k_p from D_{13} = 5.89 eV to D_{10} = 8.54 eV.

VI. Conclusion

The radiative rate constants of the carbon cations C_N^+, N = 8, 10, 13–16 have been measured and all found to be consistent with recurrent fluorescence, *i.e.* emission of radiation from thermally excited electronic states. The rate constants were all within a factor of three of 10^4 s^{-1}, in contrast to the much more disperse values based on theoretically calculated energies and oscillator strengths.

Conflicts of interest

There are no conflicts to declare.

Appendix I

The rotational partition function that enters the unimolecular decay constant in eqn (10) is calculated with the high temperature limit of a non-linear molecule:

$$Z_3 = \sqrt{\pi}\left(\frac{T}{\sigma B}\right)^{3/2}, \quad (11)$$

where $B = 1.57$ K is the geometric average of the three rotational constants of C_3 in temperature units. The symmetry number is taken to be $\sigma = 2$. We note that a treatment analogous to the one described in ref. 55 may be more suitable for the combined rotational–vibrational partition function, but parametrizing the effect with the single number 2 is well justified because of its marginal numerical consequences. The attachment cross section will be summarily set to a common value of 30 Å^2. The lesson from the studies of gas phase fullerene thermal disintegration, in particular the numerous measured kinetic energy release distributions,[56–58] gives a clear indication that attachment and collision cross sections are effectively identical, at least at the elevated temperature of the situations described here. Inserting constants then gives the dissociation rate constants

$$k_{a,N} = \left(\frac{T_d}{[\mathrm{K}]}\right)^{7/2} 9.5 \times 10^{10}\ \left[\mathrm{s}^{-1}\right] \frac{\rho_{N-3,3}(E - D_N)}{\rho_N(E)}, \qquad (12)$$

where $\rho_{N-3,3}$ is the level density of the combined vibrational degrees of freedom of the product cation and the trimer. The relatively high value of the frequency factor can be traced to the presence of the rotational partition function. This effect has been discussed in detail for fullerenes in ref. 59, and the discussion there applies equally well here, mutatis mutandis.

The level densities required for the rate constants were calculated with the Beyer–Swinehart algorithm[60] with a numerical resolution of 1 cm^{-1}, which was found sufficient. The temperature factor in eqn (12) was derived as an integral involving the logarithmic derivative of the level density. An expression which is both more precise and numerically convenient, in spite of its unwieldy appearance, is the sum

$$\begin{aligned} &T_d^{7/2}\rho_{N-3,3}(E - D_N) \\ &= \sum_{n=0}^{(E-D_N)/1\ [\mathrm{cm}^{-1}]} cn^{5/2}\rho_{N-3,3}\left(E - D_N - n\ \left[\mathrm{cm}^{-1}\right]\right), \end{aligned} \qquad (13)$$

where $c = 1.44^{5/2}$ is the conversion factor between wavenumbers and kelvin.

Appendix II

The expression for the measured decay rate with a constant photon emission rate constant is

$$I \propto \frac{e^{-k_p t}}{t}, \qquad (14)$$

with the zero of the time t defined appropriately, as explained in the main text. This expression is derived in the approximation that k_p is energy independent. As photon emission is an activated process, it will have an energy dependence, although it is weak, as shown by the numerical examples in ref. 17 and by the results calculated here. The non-zero value nevertheless makes it relevant to calculate the effect of this energy dependence.

To do so, consider the derivation of eqn (14). It results from the ensemble averaging

$$I \propto \int_0^\infty k_a e^{-(k_a + k_p)t} dE. \qquad (15)$$

For a constant k_p this simplifies to

$$I \propto e^{-k_p t} \int_0^\infty k_a e^{-k_a t} dE. \qquad (16)$$

The remaining integral is proportional to $1/t$ for any rate constant varying rapidly with energy, giving eqn (14). The interpretation of the result for a constant k_p is simple: The decay rate is given by a power law decay that arise from the averaging over the excitation energies in the ensemble. The photon emission depletes the amplitude of this energy distribution, in this approximation with an energy independent rate constant. The decay rate is therefore reduced by the corresponding reduction in this population.

For an energy dependent k_p we can then find the generalized expression by inserting the relevant energy dependent value of k_p into eqn (14);

$$I \propto \frac{e^{-k_p(E[k_a = 1/t])t}}{t}. \qquad (17)$$

To find $E(t)$, k_p is expanded in energy. A first order expansion gives

$$k_p = k_p(E_0) + \frac{dk_p}{dE}\frac{dE}{dt}\left(t - k_p(E_0)^{-1}\right). \qquad (18)$$

The result of this calculation will be a small numerical correction, and it therefore permits a calculation with a rather simple starting point for the rate constants. Using Arrhenius approximations for both k_p and k_a, as well as linear caloric curves, we get the derivative

$$\frac{k_p}{dE} = k_p \frac{h\nu C_v}{E^2}, \qquad (19)$$

where C_v is the heat capacity of the cluster in units of Boltzmann's constant. The energy of the clusters that decay at time t is with the same approximations given by

$$E = \frac{E_a C_v}{\ln(\omega_a t)}, \qquad (20)$$

where E_a is the evaporative activation energy and ω_a is the rate constant frequency factor. With this value the derivative in eqn (19) equals

$$\frac{k_p}{dE} = k_p \frac{h\nu \ln(\omega_a t)^2}{E_a^2 C_v}. \qquad (21)$$

The second derivative in eqn (18) becomes

$$\frac{dE}{dt} = \frac{d}{dt}\frac{E_a C_v}{\ln(\omega_a t)} = -\frac{E_a C_v}{t(\ln(\omega_a t))^2}. \qquad (22)$$

Inserting these results into eqn (18) gives us

$$k_p = k_p(E_0)\left(1 - \frac{h\nu}{E_a}\right) + \frac{h\nu}{E_a}\frac{1}{t}. \qquad (23)$$

This provides the first order correction from the finite slope of the k_p *vs.* E, and the decay rate becomes

$$I \propto \frac{e^{-k_p(E_0)\left(1-\frac{h\nu}{E_a}\right)t}}{t}, \quad (24)$$

where the last term in eqn (23) is absorbed into a constant. The correction therefore amounts to a minor correction before the value of the fitted parameter can be identified with the photon emission rate constant.

Acknowledgements

PF acknowledges the FWO for a post-doctoral grant. TA acknowledges the JSPS KAKENHI grant numbers 26220607. Calculations were performed at the Chalmers Centre for Computational Science and Engineering (C3SE) provided by the Swedish National Infrastructure for Computing (SNIC).

References

1 J. Zhen, S. Rodriguez Castillo, C. Joblin, G. Mulas, H. Sabbah, A. Giuliani, L. Nahon, S. Martin, J. P. Champeaux and P. M. Mayer, *Astrophys. J.*, 2016, **822**, 113.
2 A. G. G. M. Tielens, *Rev. Mod. Phys.*, 2013, **85**, 1021.
3 H. Á. Galué and G. D. Leines, *Phys. Rev. Lett.*, 2017, **119**, 171102.
4 O. Berné and A. G. G. M. Tielens, *PNAS*, 2012, **109**, 402.
5 J. Cami, J. Bernard-Salas, E. Peeters and S. E. Malek, *Science*, 2010, **329**, 1180.
6 J. K. Jørgensen, C. Favre, S. E. Bisschop, T. L. Bourke, E. F. van Dishoeck and M. Schmalzl, *Astrophys. J., Lett.*, 2012, **757**, L4.
7 A. Nitzan and J. Jortner, *J. Chem. Phys.*, 1979, **71**, 3524.
8 S. Leach, in *Polycyclic Aromatic Hydrocarbons and Astrophysics*, ed. A. Léger, L. d'Hendecourt and N. Boccara, NATO ASI Series, 1987, vol. 191, pp. 99–127, ISBN 978-94-010-8619-6.
9 A. Léger, P. Boissel and L. d'Hendecourt, *Phys. Rev. Lett.*, 1988, **60**, 921.
10 K. Hansen and E. E. B. Campbell, *J. Chem. Phys.*, 1996, **104**, 5012.
11 J. U. Andersen, C. Brink, P. Hvelplund, M. O. Larsson, B. B. Nielsen and H. Shen, *Phys. Rev. Lett.*, 1996, **77**, 3991.
12 S. Tomita, J. U. Andersen, C. Gottrup, P. Hvelplund and U. V. Pedersen, *Phys. Rev. Lett.*, 2001, **87**, 073401.
13 J. U. Andersen, C. Gottrup, K. Hansen, P. Hvelplund and M. O. Larsson, *Eur. Phys. J. D*, 2001, **17**, 189.
14 A. E. K. Sundén, M. Goto, J. Matsumoto, H. Shiromaru, H. Tanuma, T. Azuma, J. U. Andersen, S. E. Canton and K. Hansen, *Phys. Rev. Lett.*, 2009, **103**, 143001.
15 G. Ito, T. Furukawa, H. Tanuma, J. Matsumoto, H. Shiromaru, T. Majima, M. Goto, T. Azuma and K. Hansen, *Phys. Rev. Lett.*, 2014, **112**, 183001.
16 V. Chandrasekaran, B. Kafle, A. Prabhakaran, O. Heber, M. Rappaport, H. Rubinstein, D. Schwalm, Y. Toker and D. Zajfman, *J. Phys. Chem. Lett.*, 2014, **5**, 4078.
17 N. Kono, T. Furukawa, H. Tanuma, J. Matsumoto, H. Shiromaru, T. Azuma, K. Najafian, M. S. Pettersson, B. Dynefors and K. Hansen, *Phys. Chem. Chem. Phys.*, 2015, **17**, 24732.
18 Y. Ebara, T. Furukawa, J. Matsumoto, H. Tanuma, T. Azuma, H. Shiromaru and K. Hansen, *Phys. Rev. Lett.*, 2016, **117**, 133004.
19 S. Martin, J. Bernard, R. Brédy, B. Concina, C. Joblin, M. Ji, C. Ortéga and L. Chen, *Phys. Rev. Lett.*, 2013, **110**, 063003.
20 S. Martin, M. Ji, J. Bernard, R. Brédy, B. Concina, A. R. Allouche, C. Joblin, C. Ortega, G. Montagne and A. Cassimi, *et al.*, *Phys. Rev. A: At., Mol., Opt. Phys.*, 2015, **92**, 53425.
21 M. Ji, J. Bernard, L. Chen, C. Ortéga, A. Joblin, C. Cassimi and S. Martin, *J. Chem. Phys.*, 2017, **146**, 44301.
22 J. Bernard, L. Chen, R. Brédy, M. Ji, C. Ortéga, J. Matsumoto and S. Martin, *Nucl. Instrum. Methods Phys. Res., Sect. B*, 2017, **408**, 21.
23 C. Walther, G. Dietrich, W. Dostal, K. Hansen, S. Krückeberg, K. Lützenkirchen and L. Schweikhard, *Phys. Rev. Lett.*, 1999, **83**, 3816.
24 M. Lange, M. W. Froese, S. Menk, D. Bing, F. Fellenberger, M. Grieser, F. Laux, D. A. Orlov, R. Repnow and T. Sieber, *et al.*, *New J. Phys.*, 2012, **14**, 065007.
25 K. Hansen, Y. Li, V. Kaydashev and E. Janssens, *J. Chem. Phys.*, 2014, **141**, 024302.
26 K. Hansen, M. H. Stockett, M. Kamińska, R. F. Nascimento, E. K. Anderson, M. Gatchell, K. C. Chartkunchand, G. Eklund, H. Zettergren and H. T. Schmidt, *et al.*, *Phys. Rev. A*, 2017, **95**, 022511.
27 P. Ferrari, E. Janssens, P. Lievens and K. Hansen, *J. Chem. Phys.*, 2015, **143**, 224313.
28 P. Ferrari, J. Vanbuel, K. Hansen, P. Lievens, E. Janssens and A. Fielicke, *Phys. Rev. A*, 2018, **98**, 012501.
29 S. Jinno, T. Takao, K. Hanada, M. Goto, K. Okuno, H. Tanuma, T. Azuma and H. Shiromaru, *Nucl. Instrum. Methods Phys. Res., Sect. A*, 2007, **572**, 568.
30 C. H. Bae and S. M. Park, *J. Chem. Phys.*, 2002, **117**, 5347.
31 M. Goto, A. E. K. Sundén, H. Shiromaru, J. Matsumoto, H. Tanuma, T. Azuma and K. Hansen, *J. Chem. Phys.*, 2013, **139**, 054306.
32 K. Najafian, M. S. Pettersson, B. Dynefors, H. Shiromaru, J. Matsumoto, H. Tanuma, T. Furukawa, T. Azuma and K. Hansen, *J. Chem. Phys.*, 2014, **140**, 104311.
33 N. Kono, T. Furukawa, H. Tanuma, J. Matsumoto, H. Shiromaru, T. Azuma, K. Najafian, M. S. Pettersson, B. Dynefors and K. Hansen, *Phys. Chem. Chem. Phys.*, 2015, **17**, 24732.
34 K. Hansen, J. U. Andersen, P. Hvelplund, S. P. Møller, U. V. Pedersen and V. V. Petrunin, *Phys. Rev. Lett.*, 2001, **87**, 123401.
35 J. Fedor, K. Hansen, J. U. Andersen and P. Hvelplund, *Phys. Rev. Lett.*, 2005, **94**, 113201.
36 M. W. Froese, K. Blaum, F. Fellenberger, M. Grieser, M. Lange, F. Laux, S. Menk, D. A. Orlov, R. Repnow and T. Sieber, *et al.*, *Phys. Rev. A: At., Mol., Opt. Phys.*, 2011, **83**, 023202.

37 C. Breitenfeldt, K. Blaum, M. Froese, S. George, G. Guzmá-Ramírez, M. Lange, S. Menk, L. Schweikhard and A. Wolf, *Phys. Rev. A*, 2016, **94**, 033407.
38 J. U. Andersen, C. Brink, P. Hvelplund, M. O. Larsson, B. B. Nielsen and H. Shen, *Phys. Rev. Lett.*, 1996, **77**, 3991.
39 J. U. Andersen, E. Bonderup and K. Hansen, *J. Phys. B: At. Mol. Phys.*, 2002, **35**, R1.
40 R. C. Dunbar, *Mass Spectrom. Rev.*, 1992, **11**, 309.
41 K. Hansen, *Int. J. Mass Spectrom.*, 2018, **430**, 14.
42 K. Hansen, *Statistical Physics of Nanoparticles in the Gas Phase*, Springer Series on Atomic, Optical, and Plasma Physics, Springer, Dordrecht, 2nd edn, 2018, vol. 73.
43 J. Fulara, I. Shnitko, A. Batalov and J. P. Maier, *J. Chem. Phys.*, 2005, **123**, 044305.
44 F. Neese, *Wiley Interdiscip. Rev.: Comput. Mol. Sci.*, 2012, **2**, 73.
45 G. von Helden, M. T. Hsu, N. Gotts and M. T. Bowers, *J. Phys. Chem.*, 1993, **97**, 8182.
46 M. J. Frisch, G. W. Trucks, H. B. Schlegel, G. E. Scuseria, M. A. Robb, J. R. Cheeseman, G. Scalmani, V. Barone, G. A. Petersson and H. Nakatsuji, *et al.*, *Gaussian 16, Revision b.01*, 2016, Gaussian Inc., Wallingford, CT, 2016.
47 G. von Helden, P. R. Kemper, N. G. Gotts and M. T. Bowers, *Science*, 1993, **259**, 1300.
48 M. E. Geusic, T. J. Mcllrath, M. F. Jarrold, L. A. Bloomfield, R. R. Freeman and W. L. Brown, *J. Chem. Phys.*, 1986, **84**, 2421.
49 M. E. Geusic, M. F. Jarrold, T. J. McIlrath, R. R. Freeman and W. L. Brown, *J. Chem. Phys.*, 1987, **86**, 3862.
50 P. P. Radi, M. E. Rincon, M. T. Hsu, J. Brodbelt-Lustig, P. Kemper and M. T. Bowers, *J. Chem. Phys.*, 1989, **93**, 6187.
51 M. B. Sowa, P. A. Hinz and S. L. Anderson, *J. Chem. Phys.*, 1991, **95**, 4719.
52 C. Lifshitz, P. Sandler, H. F. Griitzmacher, J. Sun, T. Weiske and H. Schwartz, *J. Phys. Chem.*, 1993, **97**, 6592.
53 R. Bouyer, F. R. Monchicourt, M. Perdix and P. Pradel, *J. Chem. Phys.*, 1994, **100**, 8912.
54 K. B. Shelimov, J. M. Hunter and M. F. Jarrold, *Int. J. Mass Spectrom. Ion Processes*, 1994, **138**, 17.
55 A. Sinha and J. L. Kinsey, *J. Chem. Phys.*, 1984, **80**, 2029.
56 R. Wörgötter, B. Dünser, T. D. Märk, M. Foltin, C. E. Klots, J. Laskin and C. Lifshitz, *J. Chem. Phys.*, 1996, **104**, 1225.
57 C. Lifshitz, *Int. J. Mass Spectrom.*, 2000, **198**, 1.
58 J. Laskin and C. Lifshitz, *J. Mass Spectrom.*, 2001, **36**, 459ISSN 1096-9888.
59 K. Hansen, E. E. B. Campbell and O. Echt, *Int. J. Mass Spectrom.*, 2006, **252**, 79.
60 T. Beyer and D. F. Swinehart, *Commun. ACM*, 1973, **16**, 379, ISSN 0001-0782.